d'Collection

치의과학 박사학위논문

Automatic Diagnosis for Odontogenic Cysts and Tumors of Jaw on Panoramic Radiographs using a Deep Convolutional Neural Network

파노라마방사선영상에서 딥러닝 신경망을
이용한 치성 낭과 종양의 자동 진단 방법

2021년 2월

서울대학교 대학원

치의과학과 영상치의학 전공

권 오 득

Automatic Diagnosis for Odontogenic Cysts and Tumors of Jaw on Panoramic Radiographs using a Deep Convolutional Neural Network

지도교수 이 원 진

이 논문을 치의과학 박사학위논문으로 제출함

2020년 12월
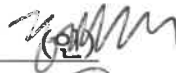
서울대학교 대학원

치의과학과 영상치의학 전공

권 오 득

권오득의 박사학위논문을 인준함

2021년 1월

위 원 장   허민석   (인)

부 위 원 장   이원진   (인)

위   원   허경희   (인)

위   원   이재성   (인)

위   원   정홍   (인)

Abstract

Automatic Diagnosis for Odontogenic Cysts and Tumors of Jaw on Panoramic Radiographs using a Deep Convolutional Neural Network

ODEUK KWON

Department of Oral and Maxillofacial Radiology

School of Dentistry

Seoul National University

Objective: The purpose of this study was to automatically diagnose odontogenic cysts and tumors of the jaw on panoramic radiographs using a deep convolutional neural network. A novel framework method of deep convolutional neural network was proposed with data augmentation for detection and classification of the multiple diseases.

Methods: A deep convolutional neural network modified from YOLOv3 was developed for detecting and classifying odontogenic

cysts and tumors of the jaw. Our dataset of 1,282 panoramic radiographs comprised 350 dentigerous cysts, 302 periapical cysts, 300 odontogenic keratocysts, 230 ameloblastomas, and 100 normal jaw with no disease. In addition, the number of radiographs was augmented 12-fold by flip, rotation, and intensity changes. The Intersection over union threshold value of 0.5 was used to obtain performance for detection and classification. The classification performance of the developed convolutional neural network was evaluated by calculating sensitivity, specificity, accuracy, and AUC (Area under the ROC curve) for diseases of the jaw.

Results: The overall classification performance for the diseases improved from 78.2% sensitivity, 93.9% specificity, 91.3% accuracy, and 0.86 AUC using the convolutional neural network with unaugmented dataset to 88.9% sensitivity, 97.2% specificity, 95.6% accuracy, and 0.94 AUC using the convolutional neural network with augmented dataset. Convolutional neural network using augmented dataset had the following sensitivities, specificities, accuracies, and AUC: 91.4%, 99.2%, 97.8%, and 0.96 for dentigerous cysts, 82.8%, 99.2%, 96.2%, and 0.92 for periapical cysts, 98.4%, 92.3%, 94.0%, and 0.97 for odontogenic keratocysts, 71.7%, 100%, 94.3%, and 0.86 for ameloblastomas, and 100.0%, 95.1%, 96.0%, and 0.94 for normal jaw, respectively.

Conclusion: The novel framework convolutional neural network method was developed for automatically diagnosing odontogenic cysts and tumors of the jaw on panoramic radiographs using data augmentation. The proposed convolutional neural network model showed high sensitivity, specificity, accuracy, and AUC despite the limited number of panoramic images involved.

Keywords: Automatic diagnosis, odontogenic cysts and tumors, panoramic radiographs, data augmentation, deep learning, deep convolutional neural network

Student Number: 2017-38170

Contents

Tables

Figure legends

Figure 1. Labeling process on a panoramic image using ImageJ

Figure 2. Data augmentation using flipping, rotation, and gamma correction.

Figure 3. A framework of the deep convolutional neural network for detection and classification of multiple diseases.

Figure 4. A convolutional neural network architecture modified from YOLOv3 with the modified layers in Bold.

Figure 5. Detection of a dentigerous cyst. The solid line area is the disease area labeled by the radiologist and the dotted area is the predicted area.

Figure 6. Detection of a periapical cyst. The solid line area is the disease area labeled by the radiologist and the dotted area is the predicted area.

Figure 7. Detection of an odontogenic keratocyst. The solid line area is the disease area labeled by the radiologist and the dotted area is the predicted area.

Figure 8. Detection of ameloblastoma. The solid line area is the disease area labeled by the radiologist and the dotted area is the predicted area.

Figure 9. Precision-recall curves from automatic detection of dentigerous cysts, periapical cysts, odontogenic keratocysts, and ameloblastomas without (a) and with (b) data set augmentation. AB, ameloblastoma; DCs, dentigerous cysts; OKCs, odontogenic keratocysts; PCs, periapical cysts.

Figure 10. Lesions annotated by the radiologist (solid line) and correctly classified by the developed convolutional neural network model (dotted line) as a dentigerous cyst (a), periapical cyst (b), odontogenic keratocyst (c), and ameloblastoma (d) without dataset augmentation. A correctly classified (solid line) dentigerous cyst (e), periapical cyst (f), odontogenic keratocyst (g), and ameloblastoma (h) with dataset augmentation, and a falsely classified (dotted line) odontogenic keratocyst (e), none (f), dentigerous cyst (g), and dentigerous cyst (h) without dataset augmentation.

Figure 11. Receiver Operating Characteristic curves from automatic classification of dentigerous cysts, periapical cysts, odontogenic keratocysts, ameloblastomas, and normal jaws without (a) and with (b) dataset augmentation.

Introduction

Panoramic radiography is an essential modality in diagnosis and treatment in the oral and maxillofacial field. In particular, it is useful for diagnosing cavities, periodontitis, bony lesions, maxillary sinus lesions, and temporomandibular joint dysfunctions, as it provides overall anatomical and pathological information on the maxillary sinus, temporomandibular joints, bone structures, and all teeth in the oral and maxillofacial region[1,2]. In dental clinics, panoramic imaging remains the most routinely applied diagnostic modality in comparison with other options such as periapical radiography, cone-beam computed tomography, magnetic resonance imaging, and ultrasound [3,4].

As general dentists are in charge of primary diagnosis and treatment in oral and maxillofacial patients in local clinics, their principal item of concern and interest is the presence of any cavities or periodontitis in radiographic readings[5]. Because of a lack of interest or expertise with diagnosis and the potential masking of lesions by superpositioning structures on panoramic radiographs, the clinician may misdiagnose or not detect lesions that require early detection and immediate surgical intervention. In dental hospitals, diagnosis using radiographic images is performed by professional oral and maxillofacial radiologists. However, the diagnosis may take too long

to finalize because of the critical shortage of experts in this field and the subspecialized nature of the dental hospital[6,7]. One of the available solutions for these problems is the further expansion of the use of computer-aided diagnosis in oral and maxillofacial imaging.

Computer-aided diagnosis has been utilized to identify cavities and periodontitis lesions as well as maxillary sinusitis, osteoporosis, and other pathologies in the oral and maxillofacial field[8]. It can provide dental professionals with a valuable second opinion by detecting and classifying pathological changes automatically. Conventional computer-aided diagnosis systems require extraction of the most significant features before training to successfully recognize or classify images, but feature extraction is a difficult and time-consuming task. A recent method based on deep learning, a subset of machine learning, can overcome this limitation by automatically extracting relevant features during training, and uses the whole image directly without best-feature representation[9-11]. Deep learning-based methods have been used extensively to solve complex problems in radiology[12]. A deep convolutional neural network, a type of deep learning, is the most commonly used method for organ segmentation[13,14] as well as classification[15,16] and detection[17,18] of organs and related diseases in medical imaging. Various attempts have been made to determine specific characteristics of target regions intended for detection and classification[19]. Research into the

applications of computer−aided diagnosis using deep convolutional neural network has been expanding rapidly, and is expected to produce more accurate diagnoses at faster rates[8].

However, application of deep learning in the field of oral and maxillofacial imaging has been limited to detection of landmarks in cephalograms[20], detection and classification of teeth[21−23], diagnosis of cavities[24−27], diagnosis of periodontitis[28], and detection of maxillary sinusitis[29]. One study aimed to achieve automatic segmentation of all teeth[21], while other research used deep learning to classify the root morphology of the mandibular first molar[30], convert a two− dimensional panoramic image to a three−dimensional one[31], and diagnose osteoporosis in panoramic radiographs[32,33].

To date, few studies have used deep learning to detect and classify radiolucent lesions in the jaw. A deep learning object detection technique was used for automatic detection and classification of radiolucent lesions in the mandible[34], and for differential diagnosis between ameloblastomas and odontogenic keratocysts of the jaw on panoramic radiographs[35]. Precise preoperative diagnosis of these tumors and cysts of the jaw can help oral and maxillofacial surgeons plan appropriate treatment, but this is more difficult in the maxilla than in the mandible because of superimposition of the normal structures in the maxilla[36]. Nonetheless, no study to date has examined the functionality of deep convolutional neural network for automatic

3

diagnosis of odontogenic cysts and tumors occurring in the jaw using panoramic radiographs.

In order, first is the periapical cyst, which develops and proliferates from the epithelial cell rests of Malassez in the periodontal ligament through inflammatory stimulation of infected tooth tissue[37,38]. Second is the dentigerous cyst, the most common form of developmental odontogenic cysts, which originates from the separation of the tooth follicle and the crown of an unerupted tooth[39,40]. Next are odontogenic keratocysts. Unlike other cysts enlarged solely by osmosis, these are filled with highly viscous keratin from the epithelium and have the highest recurrence among odontogenic cysts[41,42]. Last are ameloblastomas, the most common, clinically significant neoplasms of the odontogenic epithelium that—though benign—display locally invasive growth characteristics[43-45].

Therefore, the purpose of this study was to automatically diagnose odontogenic cysts and tumors of the jaw with the highest rate of occurrence in the oral and maxillofacial regions. A novel framework of deep convolutional neural network was proposed with data augmentation for detection and classification of the multiple diseases.

Materials and Methods

Data preparation and augmentation of panoramic radiographs

A total of 1,282 panoramic radiographs of patients who visited Seoul National University Dental Hospital from 1999 to 2017 was prepared. The panoramic radiographs of each patient were acquired using a dental panoramic X-ray machine (Orthopantomograph OP 100D, Instumentarium corporation, Tuusula, Finland) at Seoul National University Dental Hospital. These radiographs included 350 dentigerous cysts (273 in the mandible and 77 in the maxilla), 302 periapical cysts (123 in the mandible and 179 in the maxilla), 300 odontogenic keratocysts (266 in the mandible and 34 in the maxilla), and 230 ameloblastomas (222 in the mandible and eight in the maxilla) (Table 1). As a control group, 100 normal panoramic radiographs were also prepared. Panoramic radiographs were obtained from adult patients without mixed dentition, and only one radiograph was used per patient. The study was approved by the Institutional Review Board (IRB) of Seoul National University Dental Hospital (ERI18001).

The cysts and tumors were classified finally based on the histopathologic diagnosis from biopsies in addition to clinical diagnosis, and panoramic radiographs were selected with the same radiologic

diagnosis by two radiologists with more than 15 years of experience. In other words, it was only used the panoramic radiographs with identical radiological and histopathological diagnoses. Panoramic radiographs had a resolution of 1,976×976 pixels(295mm × 145mm), and each radiograph was labeled manually by drawing rectangular bounding boxes around the lesions using ImageJ[46] for training(Figure 1). The bounding boxes included radiographic characteristics of each disease such as cortical margin and internal radiolucent lesions. Average sizes of the annotated lesions were 178×196 pixels for dentigerous cysts, 186×170 pixels for periapical cysts, 297×304 pixels for odontogenic keratocysts, and 386×351 pixels for ameloblastomas. A contrast−limited adaptive histogram equalization (CLAHE) technique was applied to the images to expand the high values and compress the values in the dark layer more effectively[35].

	panoramic image	augmented data	average lesion size (pixels)
dentigerous cyst	350	4200	178×196
periapical cyst	302	3624	186×170
odontogenic keratocyst	300	3600	297×304
ameloblastoma	230	2760	386×351

Table 1. The number of panoramic images and augmented data for four diseases, and average lesion size (pixels)
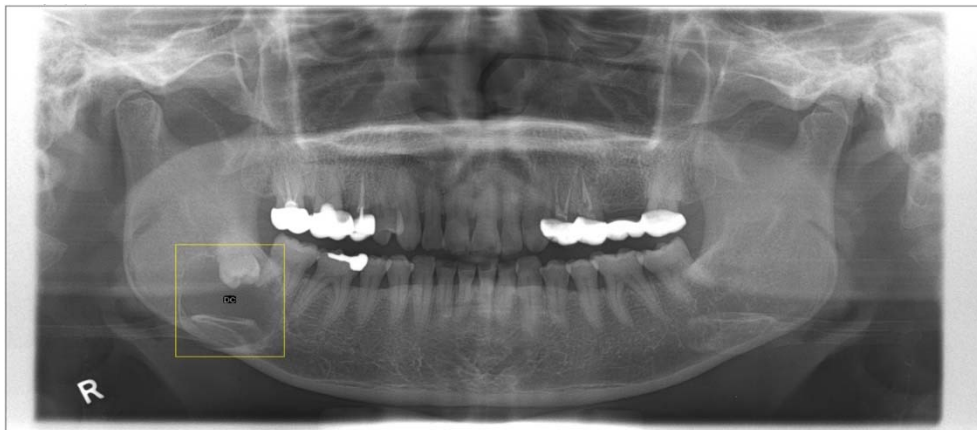

Figure 1. Labeling process on a panoramic image using ImageJ
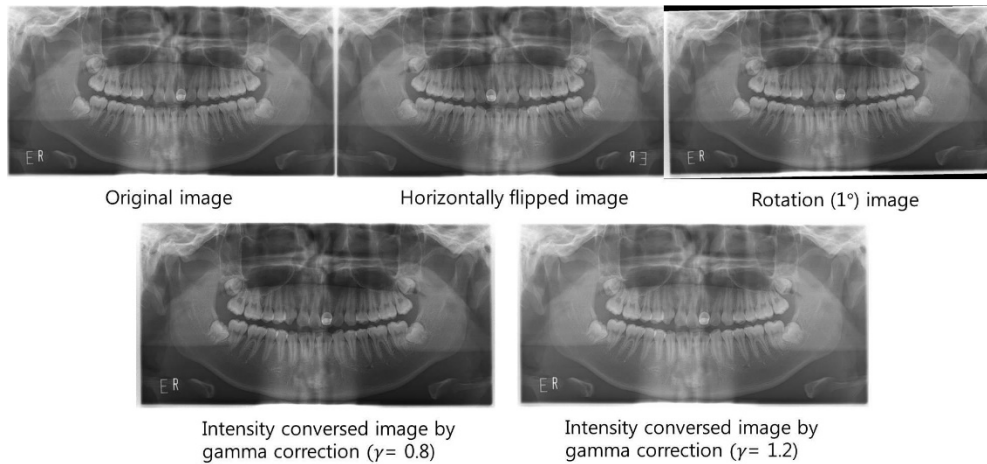
Figure 2. Data augmentation using flipping, rotation, and gamma correction.

Data augmentation was performed to increase the amount of training data for deep learning. Using MATLAB (MathWorks, Natick, MA, USA), images were flipped horizontally, rotated by 1° and −1°, and their grayscale was transformed by gamma correction (γ = 0.8, 1, 1.2) (Figure 2). As a result, the number of images was increased 12-fold. Images were randomly separated into a training dataset (80%) and a test dataset (20%) before data augmentation. The training dataset for dentigerous cyst, periapical cyst, odontogenic keratocyst, and ameloblastoma comprised 280, 242, 240 and 184 panoramic images, respectively, and test dataset, 70, 60, 60, and 46, respectively. The training dataset was used to train the convolutional neural network, and the test dataset was used to evaluate the final trained model.

8

A deep convolutional neural network model for detection and classification of multiple diseases – YOLOv3

A modified convolutional neural network from the YOLOv3 based on the Darknet-53 network for detecting and classifying multiple diseases on panoramic radiographs was developed (Figure 3). YOLOv3 predicted bounding boxes at three different scales using features from scales extracted using a similar concept to feature pyramid networks (FPN)[47]. In the last of these layers, the convolutional neural network replaced the softmax function with independent logistic classifiers to calculate the objectness of the input belonging to a specific class[48]. The convolutional neural network predicted the bounding box, confidence (objectness), and class predictions (Figure 3). Each bounding box had a confidence value calculated from the logistic regression. The input resolution from 320 × 320 pixels to 608 × 608 pixels, which made it possible to predict lesions of smaller pixel sizes, was modified. The location of skip connection was also changed from the convolutional layers of 76x76x256 to 76x76x256 to those of 152x152x128 to 152x152x128 in order to use four times up-sampling instead of two times for reducing the losses of spatial information (Figure 4). The network was trained on a total of 8,000 epochs with a 64-batch size and one-

or two-stride size by using pre-prepared augmented images. An adaptive moment estimation solver was used to optimize the network with a learning rate of 0.001 and momentum of 0.9.

After training, the network outputted bounding boxes and the confidence that the bounding box enclosed a lesion for input panoramic images. Intersection over union score, ratio of the area of intersection and area of union of the predicted bounding box and ground truth bounding box, was computed in the final set of outputs. The intersection over union threshold value of 0.5 was used to obtain the average precision score for disease detection (Figure 3). The network could detect one or more bounding boxes of possible classes for one lesion at the input panoramic image. If multiple bounding boxes of the same class were generated for one lesion, only one bounding box among the boxes was predicted for the class by non-maximum suppression. Finally, one bounding box of the highest confidence among the multiple predictions was adopted for disease classification (Figure 3).
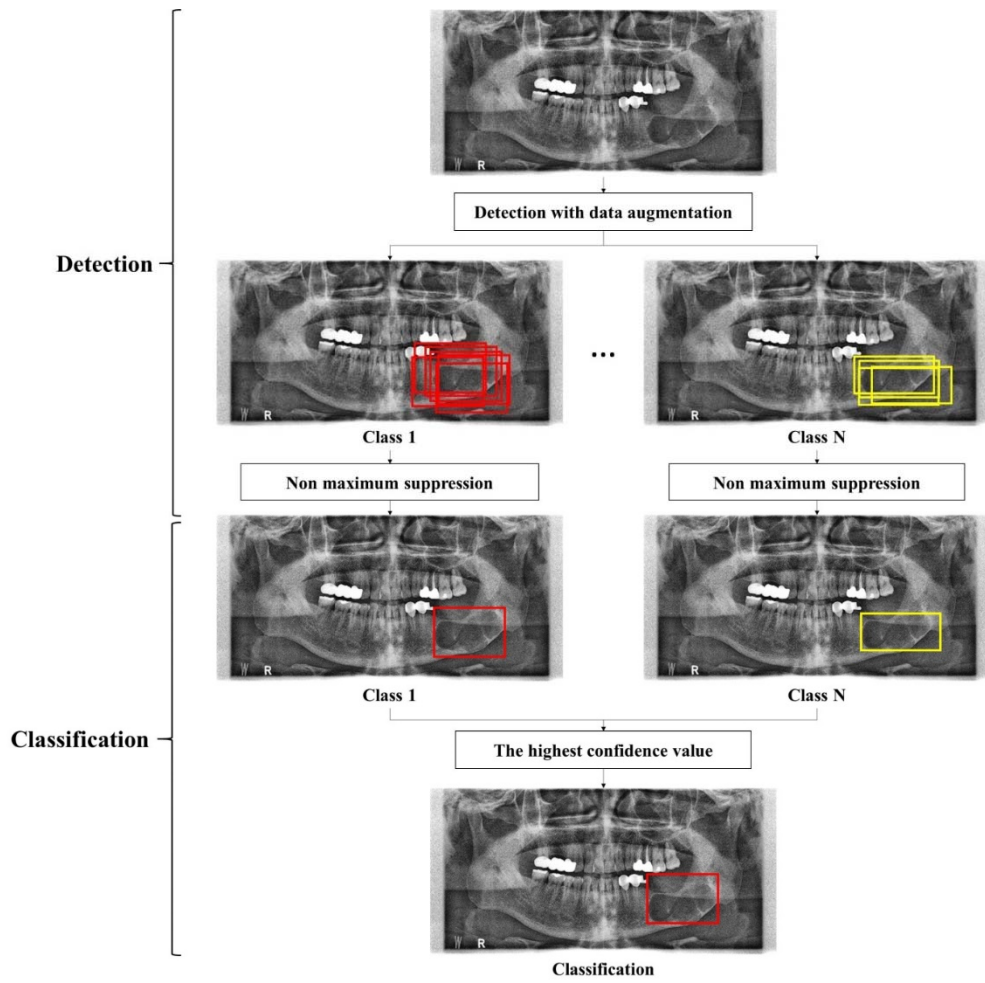
Figure 3. A framework of the deep convolutional neural network for detection and classification of multiple diseases.
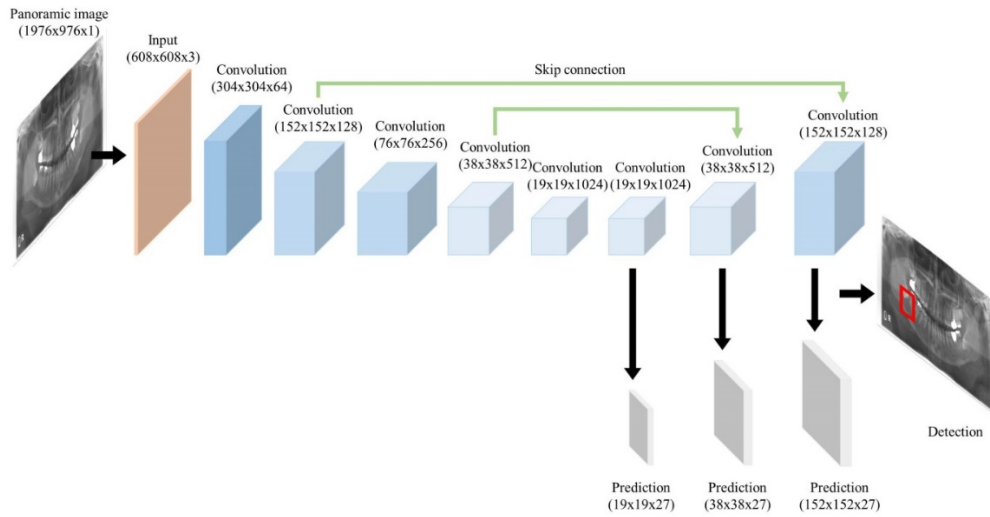
Figure 4. A convolutional neural network architecture modified from YOLOv3 with the modified layers in Bold.

Evaluation of detection and classification performance of the deep convolutional neural network model

The performance of the developed model was evaluated by five‐fold cross validation method, which divided the whole data into five sets, takes 80% for training and 20% for testing, and then rotated the two groups five times. The performance of the developed model was evaluated using a test data set not used for training. For detection performance, it was calculated recall (sensitivity) (TP / (FN + TP)), precision (positive predictive value) (TP / (FP + TP)), F1‐score (2×precision×recall / (precision + recall)), and average precision values, which are common parameters in object detection[49,50]. The precision‐recall curve (PRC) was also computed from the model's detection output by varying the confidence threshold that determined what was counted as a model‐predicted positive detection[49]. average precision was calculated as the average value of precision across all recall values. A confusion matrix was calculated to evaluate the classification performance of the convolutional neural network for diseases[51]. For classification performance, it was calculated sensitivity (TP / (FN + TP)), specificity (TN / (TN + FP)), and accuracy ((TN + TP)/(TN+TP+FN+FP)) from the confusion matrix. The receiver operating characteristic curve (ROC) was also computed

from the model's classification output by varying the confidence threshold for each disease[52]. The value of the area under the ROC curve (AUC) was calculated.

Results

First, average precision, precision and recall were measured to evaluate model performance for lesion detection with data augmentation. Figure 5 features a dentigerous cyst, with a crown, radiolucent lesion, and surrounding cortical bony margin detected.

Figure 5. Detection of a dentigerous cyst. The solid line area is the disease area labeled by the radiologist and the dotted area is the predicted area.

Figure 6 displays a periapical cyst. The enclosed area around the cyst includes a root apex, radiolucent lesion and surrounding cortical bony lesion.

Figure 6. Detection of a periapical cyst. The solid line area is the disease area labeled by the radiologist and the dotted area is the predicted area.

Figure 7 relay the results for the odontogenic keratocyst. The unilocular radiolucent cystic lesion is located to the left of the upper inferior alveolar nerve, closer to the periapical region and away from the cementoenamel junction (CEJ) of the third molar.
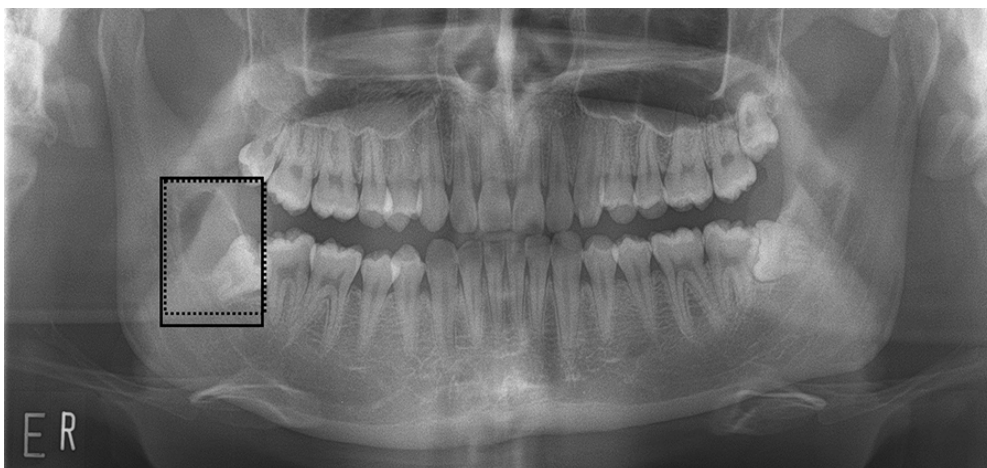
Figure 7. Detection of an odontogenic keratocyst. The solid line area is the disease area labeled by the radiologist and the dotted area is the predicted area.

Lastly, for ameloblastoma (Figure 8), the panoramic image reveals a large unilocular lesion on the maxilla's left anterior side.

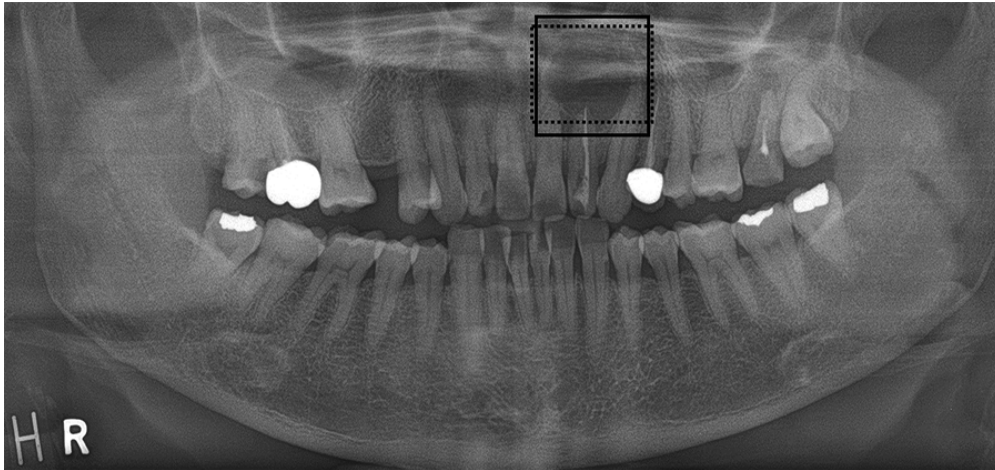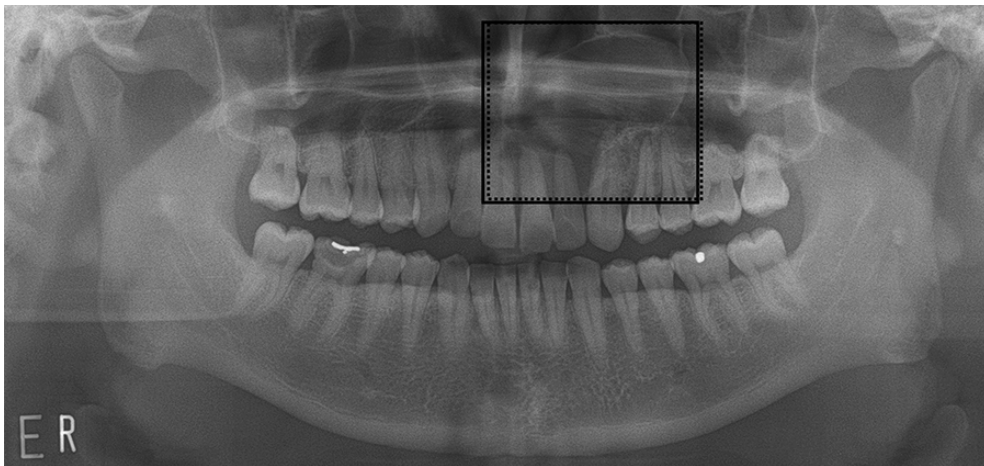

Figure 8. Detection of ameloblastoma. The solid line area is the disease area labeled by the radiologist and the dotted area is the predicted area.

Average precision, precision, recall, and F1-score values were measured to evaluate model performance for lesion detection with or without data augmentation using YoLoV3(Table 2). average precision values for dentigerous cysts, periapical cysts, odontogenic keratocysts, and ameloblastomas using non-augmented dataset were 0.91, 0.79, 0.67, and 0.78, respectively, compared to 0.84, 0.89, 0.91,

1 7

and 0.88, for augmented dataset, respectively (Table 2). Mean average precision, precision, recall, and F1-score for dentigerous cysts, periapical cysts, odontogenic keratocysts, and ameloblastomas were 0.79, 0.78, 0.74, and 0.76 for non-augmented dataset and 0.88, 0.87, 0.83, and 0.85 for augmented dataset, respectively (Table 2). The precision-recall (PR) curves for detecting lesions are shown in Figure 9.

	AP				Mean AP	Precision	Recall	F1-score
	DC	PC	OKC	AB				
With augmentation	0.84	0.89	0.91	0.88	0.88±0.04	0.87	0.83	0.85
Without augmentation	0.91	0.79	0.67	0.78	0.79±0.12	0.78	0.74	0.76

Table 2. Average precision (AP), mean average precision (mAP), precision (positive predictive value), recall (sensitivity), and F1-score for detecting dentigerous cysts (DC), periapical cysts (PC), odontogenic keratocysts (OKC), and ameloblastomas (AB) of the developed convolutional neural network with or without dataset augmentation.
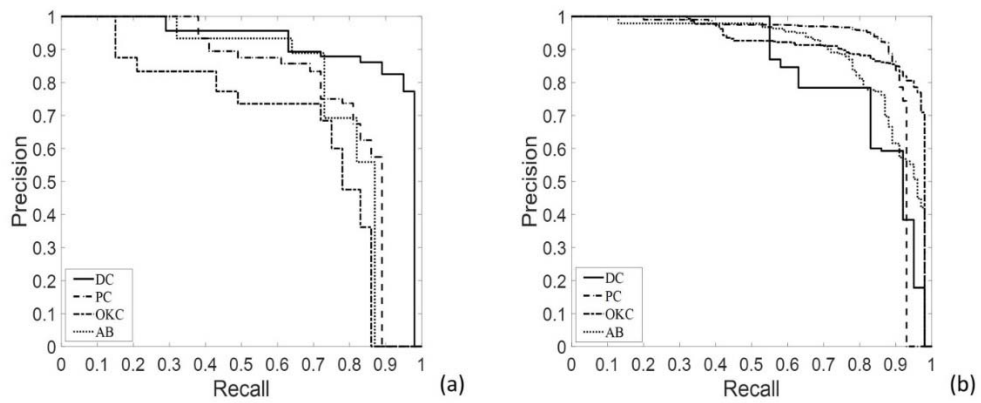
Figure 9. Precision-recall curves from automatic detection of dentigerous cysts, periapical cysts, odontogenic keratocysts, and ameloblastomas without (a) and with (b) data set augmentation. AB, ameloblastoma; DCs, dentigerous cysts; OKCs, odontogenic keratocysts; PCs, periapical cysts.

Table 3 shows the confusion matrix for classifying dentigerous cysts, periapical cysts, odontogenic keratocysts, ABs, and normal jaws using the developed convolutional neural network with or without data augmentation. To assess the classification performance of the convolutional neural network for absence of diseases, panoramic radiographs with no diseases were designated normal. Table 4 summarizes the classification results of sensitivity, sensitivity, accuracy, and AUC for each disease.

Input	Without augmentation					With augmentation				
	DC	PC	OKC	AB	Normal	DC	PC	OKC	AB	Normal
DC	0.87	0.05	0.03	0.00	0.05	0.92	0.03	0.03	0.00	0.03
PC	0.06	0.72	0.08	0.00	0.14	0.03	0.84	0.04	0.00	0.10
OKC	0.06	0.06	0.78	0.03	0.06	0.00	0.00	0.98	0.00	0.02
AB	0.05	0.05	0.27	0.55	0.09	0.00	0.00	0.22	0.72	0.06
Normal	0.00	0.00	0.01	0.00	0.99	0.00	0.00	0.00	0.00	1.00

Table 3. Confusion matrix for classifying dentigerous cysts (DC), periapical cysts (PC), odontogenic keratocysts (OKC), ameloblastomas (AB), and normal jaws (Normal) by the developed convolutional neural network, with or without dataset augmentation.

	Without augmentation				With augmentation			
	Sensitivity (%)	Specificity (%)	Accuracy (%)	AUC	Sensitivity (%)	Specificity (%)	Accuracy (%)	AUC
DC	87.1	94.7	94.1	0.91	91.4	99.2	97.8	0.96
PC	71.9	95.0	91.2	0.84	82.8	99.2	96.2	0.92
OKC	78.9	89.4	87.8	0.83	98.4	92.3	94.0	0.97
AB	54.3	99.1	90.3	0.77	71.7	100.0	94.3	0.86
Normal	99.0	91.1	92.9	0.94	100.0	95.1	96.0	0.97
Mean	78.2	93.9	91.3	0.86	88.9	97.2	95.6	0.94

Table 4. Sensitivity, specificity, accuracy, and area under the curve (AUC) for classifying dentigerous cysts (DC), periapical cysts (PC), odontogenic keratocysts (OKC), ameloblastomas (AB), and normal jaws (Normal) by the developed convolutional neural network, with or without dataset augmentation.

Figure 10 shows the correctly and falsely classified lesions with and without dataset augmentation. The receiver operating characteristic (ROC) curves for classifying multiple diseases are shown in Figure 11. For dentigerous cysts, lesions correctly classified by the convolutional neural network had a crown, radiolucent lesion, and surrounding cortical bony margin both without (Figure 10 (a)) and with data augmentation (Figure 10 (e)). Sensitivity, specificity, accuracy, and AUC for dentigerous cysts without augmentation were 87.1%, 94.7%, 94.1% and 0.91, respectively, compared to 91.4%, 99.2%, 97.8%, and 0.96, respectively, with augmentation. For periapical cysts, correctly classified lesions had a root apex, radiolucent lesion, and surrounding cortical bony lesion both without (Figure 10 (b)) and with data augmentation (Figure 10 (f)). Sensitivity, specificity, accuracy, and AUC for periapical cysts were 71.9%, 95.0%, 91.2%, and 0.84, respectively, without augmentation, and 82.8%, 99.2%, 96.2%, and 0.92, respectively, with augmentation. For odontogenic keratocysts, correctly classified lesions were unilocular radiolucent cystic lesions associated with the third molar on the mandible without augmentation (Figure 10 (c)) and large radiolucent cystic lesions extending from the border of the maxilla with augmentation (Figure 10 (g)). Sensitivity, specificity, accuracy, and AUC for odontogenic keratocysts without augmentation were 78.9%, 89.4%, 87.8%, and 0.83, respectively, compared to 98.4%,

92.3%, 94.0%, and 0.97, respectively, with augmentation. Ameloblastomas were presented as large unilocular lesions on the maxilla's anterior side without augmentation (Figure 10 (d)), and radiolucent lesions including the crown of the third molar with teeth root resorption on the mandible with augmentation (Figure 10 (h)). Sensitivity, specificity, accuracy, and AUC of the convolutional neural network for ameloblastomas was 54.3%, 99.1%, 90.3%, and 0.77, respectively, without augmentation, and 71.7%, 100%, 94.3%, and 0.86, respectively, with augmentation. Lastly, sensitivity, specificity, accuracy, and AUC for normal jaws was 99.0%, 91.1%, 92.9% and 0.94, respectively, without augmentation, and 100%, 95.1%, 96.0% and 0.97, respectively, with augmentation. Mean sensitivity, specificity, accuracy, and AUC for all diseases were 78.2%, 93.9%, 91.3%, and 0.86, respectively, without augmentation, and 88.9%, 97.2%, 95.6%, and 0.94, respectively, with augmentation.

Figure 10. Lesions annotated by the radiologist (solid line) and correctly classified by the developed convolutional neural network model (dotted line) as a dentigerous cyst (a), periapical cyst (b), odontogenic keratocyst (c), and ameloblastoma (d) without dataset augmentation. A correctly classified (solid line) dentigerous cyst (e), periapical cyst (f), odontogenic keratocyst (g), and ameloblastoma (h) with dataset augmentation, and a falsely classified (dotted line) odontogenic keratocyst (e), none (f),

2 5

dentigerous cyst (g), and dentigerous cyst (h) without dataset

augmentation.

Figure 11. Receiver Operating Characteristic curves from automatic classification of dentigerous cysts, periapical cysts, odontogenic keratocysts, ameloblastomas, and normal jaws without (a) and with (b) dataset augmentation.
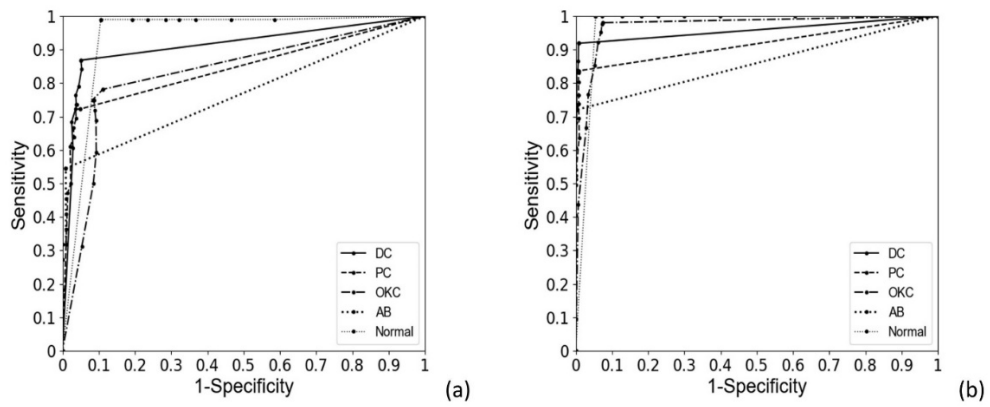
Discussion

A deep convolutional neural network, a type of deep learning model, automatically and adaptively learns spatial hierarchies of image features by using multiple building blocks of convolutional layers, pooling layers, and fully connected layers[9-11]. Various imaging modalities, such as periapical, cephalometric, panoramic radiographs, as well as cone-beam computed tomography have been used to detect and classify diseases in computer-aided diagnosis studies using a deep convolutional neural network. One study involved segmentation of teeth on panoramic images[23]. Another evaluated the root morphology of the mandibular first molar on panoramic radiography[30]. Sinusitis was detected by learning the form of the maxillary sinus on panoramic images[30]. Osteoporosis has also been diagnosed by evaluating cortical erosion of the mandibular inferior cortex from panoramic images[32]. However, there are few convolutional neural network -based computer-aided diagnosis studies of radiolucent jaw lesions on panoramic radiographs.

A modified convolutional neural network from YOLOv3 for automatically detecting and classifying odontogenic cysts and tumors of the jaw on panoramic images was developed, as these types of cysts and tumors have the highest rate of occurrence in the oral and maxillofacial region. The input resolution of the panoramic image was

increased, and the skip connections compared with the original YOLOv3 was changed, which could reduce information loss during training, and increase the performance the convolutional neural network. The developed convolutional neural network based on YOLOv3 showed overall detection performance of 0.88 of average precision, 0.87 of precision, and 0.83 of recall. Classification sensitivity was 72% for ameloblastomas, 98% for odontogenic keratocysts, 91% for dentigerous cysts, and 83% for periapical cysts using augmented dataset. A study reported automatic classification of ameloblastomas, odontogenic keratocysts, dentigerous cysts, RCs, and SBCs using DIGITS, a pre-trained deep learning model[34]. In the study, the total number of training dataset was 210, and the number of test dataset was three ameloblastomas, six odontogenic keratocysts, eight dentigerous cysts, and seven radicular cysts to evaluate the performance[34]. As the result, classification sensitivity was 60% for ameloblastomas, 13% for odontogenic keratocysts, 82% for dentigerous cysts, and 77% for RCs[34]. On the other hand, a total of 1,282 panoramic radiographs was used and data augmentation of 12 times. Generally, our convolutional neural network model showed higher sensitivities for these diseases than the model of Ariji et al., most likely because these authors used a smaller number of cysts and tumor images than we did for training and evaluation. In addition to this, odontogenic cysts and tumors in both the maxilla and mandible

2 9

was classified, while they only classified cysts and tumors in the mandible[34]. Another study reported binary classification of ameloblastomas and odontogenic keratocysts using a VGG-16 convolutional neural network, a pre-trained network using ImageNet. The number of original training dataset and test dataset was 200 and 50, respectively, for each disease. They used data augmentation of double using only horizontal flips for training dataset, and the sensitivity and specificity for differential diagnosis was 81.8%, and 83.3%, respectively[35]. In our study, the sensitivity and specificity for ameloblastomas were 71.7%, and 100%, respectively, while that for odontogenic keratocysts was 98.4%, and 92.3%, respectively. Overall sensitivity was 88.9% and overall specificity was 97.2% using data augmentation in spite of multiple classification for four diseases. Generally, the deep learning model developed based on the state-of-the-art network YOLOv3 and augmented dataset had higher sensitivity and specificity than those of previous models in classifying cysts and tumors of the jaw on panoramic images.

Odontogenic cysts and tumors classified in this study share some radiologic features, thus differential diagnosis may be difficult[53]. It is common for dentigerous cysts to wrap around the crown symmetrically, and it should not come into contact with the root as it originates from the cementoenamel junction of the crown. If a cyst arising from the crown of an unerupted tooth extends towards the

periapical side over the cementoenamel junction of the unerupted tooth, then it is likely an odontogenic keratocysts[54]. Separately, multilocular odontogenic keratocysts with scalloped borders may appear similar to ameloblastomas, but they tend to grow along the marrow space without significant cortical bone expansion compared to ameloblastomas, which usually show significant cortical expansion with well-defined cortical borders in the mandible and ill-defined margins in the maxilla[55]. It is more difficult to diagnose these radiolucent lesions correctly in the maxilla than in the mandible because of superimposition of structures such as the nasal cavity, maxillary sinus, hard palate, and inferior nasal concha in the maxilla[36].

Our convolutional neural network had 88.9% sensitivity for classification using augmented dataset. It had a 100% sensitivity (false negative rate of 0) for classification of disease-free (normal) jaws. The sensitivity for odontogenic keratocysts was the highest at 98.4% (lowest false negative rate of 0.02) among the four diseases; the false negative was classified as normal. In contrast, the lowest sensitivity of 71.7% (highest false negative rate of 0.28) was obtained for ameloblastomas among the four diseases, with false diagnosis of ameloblastomas as odontogenic keratocysts (0.22) and normal (0.06). Fewer images were used for ameloblastomas learning than for the other three diseases, despite their heterogeneous radiographic appearance (multilocular and unilocular). The second highest

sensitivity of 91.4% (false negative rate of 0.09) was obtained for dentigerous cysts among the four diseases, and dentigerous cysts were falsely diagnosed as periapical cysts (0.03), odontogenic keratocysts (0.03), or normal (0.03). dentigerous cyst lesions involving the third molar in the maxilla, those associated with the supernumerary tooth in the anterior maxilla, or those that overlapped with the wall of the maxillary sinus or anterior teeth were misdiagnosed. The sensitivity for periapical cysts was 82.8% (false negative rate of 0.17). Our model failed to diagnose smaller lesions in the root apex of the tooth overlapping with other anatomical structures (0.1), and misdiagnosed them as dentigerous cysts (0.03) or odontogenic keratocysts (0.04), especially in the maxilla. As a result, sensitivities for dentigerous cysts and periapical cysts were lower than that for odontogenic keratocysts as dentigerous cysts, and periapical cysts occur more commonly in the maxilla. Generally, sensitivity (false negative rate) for lesions located in the maxilla was lower (higher) than that for lesions in the mandible due to the overlap between lesions and other anatomical structures in the maxilla.

The classification specificity of 97.2% when using augmented dataset was higher than the sensitivity of 88.9% for all diseases. Specificity for ameloblastomas was the highest (lowest false positive rate) at 100% (0.00); no diseases were falsely diagnosed as ameloblastomas. Specificity for dentigerous cysts and periapical cysts

was also high at 99.2%. Specificity for odontogenic keratocysts was lowest at 92.3%. Ameloblastomas were frequently misdiagnosed as odontogenic keratocysts, and the classification was least sensitive for ameloblastomas. This might be due to the smaller number of ameloblastomas used for learning compared with all the other cystic diseases in addition to the large variations in radiological appearance of ameloblastomas. Rectangular bounding boxes around the lesions should have included more normal anatomical structures to cover the larger boundary of ameloblastomas. As a result, our model showed poorer generalizability for ameloblastomas than the other cystic diseases. Nonetheless, our model showed high sensitivity for odontogenic keratocysts and high specificity for ameloblastomas. It is important to note that differential diagnosis between odontogenic keratocysts and ameloblastomas based on panoramic radiographs can be difficult even for experienced radiologists.

Transfer learning is another effective way to train a network with a small dataset in radiology research. In transfer learning, a network trained previously on a large number of images such as an ImageNet challenge dataset is applied to the specific task of interest. The basic assumption of transfer learning is that the generic features learned from a sufficiently large dataset can be shared with seemingly disparate datasets. the learned kernels were utilized and the pretrained network was weighted from model of Darknet-53 and

33

fine-tuned all of the kernels of the YOLOv3 network on the pretrained convolutional base. With this strategy, the network learned specific features that were more specialized for lesion detection on the radiograph dataset progressively, while the generic features such as edges and corners could be applicable to a variety of datasets[56,57]. The advantage of reusing learned generic features makes the deep convolutional neural network very useful in various tasks with small datasets in medical and dental imaging.

An essential requirement for deep learning detection and classification of lesions on medical and dental images is large sets of accurately labeled data. However, large collections of images labeled manually by experts are not easily available in many situations. In our study, the panoramic images used herein were labeled by experienced oral and maxillofacial radiologists and matched with the histopathologic findings from the lesion biopsy. For evaluating the deep learning model with the limited image samples, the k-fold cross-validation method has been used to accurately estimate the performance of the deep learning model on images not used for training[57]. The method generally resulted in a less biased estimate of the model performance than did one simple split of train and test[58]. Using the five-fold cross-validation method, it was measured how accurately the developed model predicted when used to make predictions on unseen images.

Overfitting of the training convolutional neural network model, which results in the model learning statistical regularity specific to the training data set, negatively impacts the model's ability to generalize to a new data set[9]. One solution to reduce overfitting is data augmentation, which is the process of modifying data through flipping, moving, cropping, rotating, and grayscale transformation[59]. Data augmentation can improve the performance of the convolutional neural network in medical image analysis[59]. In this study, augmented technology increased the number of images in the dataset by 12-fold. Mean average precision, precision, recall, and F1-score values for detection performance of the convolutional neural network generally increased after data augmentation. As the recall value increased, the precision value decreased more gradually with data augmentation than without data augmentation, which resulted in a higher average precision with data augmentation than without data augmentation. Classification performance of the convolutional neural network improved from 78.2% sensitivity, 93.9% specificity, 91.3% accuracy, and 0.86 AUC to 88.9% sensitivity, 97.2% specificity, 95.6% accuracy, and 0.94 AUC for the four diseases when augmented dataset was used. As the false positive rates increased, the sensitivity increased more steeply with data augmentation than without data augmentation, which resulted in a higher AUC with data augmentation than without data augmentation. In particular, the performance for diagnosing

3 5

odontogenic keratocysts improved from 78.9% sensitivity, 89.4% specificity, 87.8% accuracy, and 0.83 AUC to 98.4% sensitivity, 92.3% specificity, 94.0% accuracy, and 0.97 AUC, and the performance for ameloblastomas from 54.3% sensitivity, 99.1% specificity, 90.3% accuracy, and 0.77 AUC to 71.7% sensitivity, 100% specificity, 94.3% accuracy, and 0.86 AUC.

To date, oral and maxillofacial medicine has benefited little from advancements in computer-aided diagnosis. Here, A convolutional neural network model to automatically detect and classify cysts and tumors of the jaw on panoramic radiographs with high accuracy using data augmentation was developed. The developed computer-aided diagnosis can help general dental clinicians diagnose and treat patients more efficiently, and thus improve diagnostic performance and patient care. In future studies, the use of a more complex annotation method, such as lesion segmentation rather than a rectangular bounding box, and the use of more images for training, especially images of the maxilla, will increase the classification performance of the convolutional neural network for diseases of the jaw.

Conclusion

The convolutional neural network method was developed for automatically diagnosing odontogenic cysts and tumors of the jaw on panoramic radiographs using data augmentation. The proposed convolutional neural network model showed high sensitivity, specificity, accuracy, and AUC when using augmented data despite the limited number of panoramic images available.

Acknowledgments

References

1. Barrett AP, Waters BE, Grifiths Cri CJ. A critical evaluation of panoramic radiography as a screening procedure in dental practice. Oral Surg Oral Med Oral Pathol 1984;57: 673-677.

2. Kantor ML, Slome BA. Efficacy of panoramic radiography in dental diagnosis and treatment planning. J Dent Res 1989;68: 810–812.

3. White SC, Pharoah MJ. The evolution and application of dental maxillofacial imaging modalities. Dent Clin N Am 2008;52: 689–705.

4. H.P. van tien Akker. Diagnostic imaging in salivary gland disease. Oral Surg Oral Med Oral Pathol 1988;66: 625–37

5. Douglass CW, Valachovic RW, Wijesinha A, Chauncey HH, Kapur KK, McNeil BJ. Clinical efficacy of dental radiography in the detection of dental caries and periodontal diseases. Oral Surg Oral Med Oral Pathol 1986;62: 330–339

6. Dare A, Yamaguchi A, Yoshiki S, Okano T. Limitation of panoramic radiography in diagnosing adenomatoid odontogenic tumors. Oral Surg Oral Med Oral Pathol 1994;77: 662–668.

7. Ohba T. Value and limitation of panoramic radiography in the diagnosis of maxillary sinus pathosis. Int J Oral Maxillofac Surg 1977;6 211–214.

8. Wang CW, Huang CT, Lee JH, Li CH, Chang SW, Siao MJ, et al. A benchmark for comparison of dental radiography analysis

3 9

algorithms. Med Image Anal 2016;31: 63-76.

9. Yamashita R, Nishio M, Do RKG, Togashi K. Convolutional neural networks: an overview and application in radiology. Insights Imaging 2018;9: 611-629.

10. Yonekura A, Kawanaka H, Prasath VBS, Aronow BJ, Takase H. Automatic disease stage classification of glioblastoma multiforme histopathological images using deep convolutional neural network. Biomed Eng Lett 2018;8: 321-327.

11. Billah M, Waheed S. Gastrointestinal polyp detection in endoscopic images using an improved feature extraction method. Biomed Eng Lett 2018;8:69-75.

12. Schmidhuber J. Deep learning in neural networks: An overview. Neural Networks 2015;61:85-117.

13. Kallenberg M, Petersen K, Nielsen M, Ng AY, Diao PF, Igel C, et al. Unsupervised Deep Learning Applied to Breast Density Segmentation and Mammographic Risk Scoring. IEEE T Med Imaging 2016;35:1322-1331.

14. Zhao XM, Wu YH, Song GD, Li ZY, Zhang YZ, Fan Y. A deep learning model integrating FCNNs and CRFs for brain tumor segmentation. Med Image Anal 2018;43:98-111.

15. Esteva A, Kuprel B, Novoa RA, Ko J, Swetter SM, Blau HM, et al. Dermatologist-level classification of skin cancer with deep neural networks. Nature 2017;542:115-118.

16. Gao XHW, Hui R, Tian ZM. Classification of ct brain images based on deep learning networks. Comput Meth Prog Bio 2017;138:49-56.

17. Teramoto A, Fujita H, Yamamuro O, Tamaki T. Automated detection of pulmonary nodules in PET/CT images: Ensemble false-positive reduction using a convolutional neural network technique. Med Phys 2016;43:2821-2827.

18. Hannun AY, Rajpurkar P, Haghpanahi M, Tison GH, Bourn C, Turakhia MP, et al. Cardiologist-level arrhythmia detection and classification in ambulatory electrocardiograms using a deep neural network. Nature Medicine 2019;25:530.

19. Krizhevsky A, Sutskever I, Hinton GE. ImageNet classification with deep convolutional neural networks. Proceedings of the 25th International Conference on Neural Information Processing Systems 2012;1:1097-105.

20. Lee H, Park M, Kim J. Cephalometric landmark detection in dental x-ray images using convolutional neural networks. Medical Imaging 2017;10134:101341W.

21. Ronneberger O, Fischer P, Brox T. Dental X-ray image segmentation using a U-shaped Deep Convolutional network. International Symposium on Biomedical Imaging 2015:1-13.

22. Miki Y, Muramatsu C, Hayashi T, Zhou XR, Hara T, Katsumata A, et al. Classification of teeth in cone-beam CT using deep

convolutional neural network. Comput Biol Med 2017;80:24-29.

23. Jader G, Fontineli J, Ruiz M, Abdalla K, Pithon M, Oliveira L. Deep instance segmentation of teeth in panoramic x-ray images. 2018 31st SIBGRAPI Conference on Graphics, Patterns and Images (SIBGRAPI) 2018:400-407.

24. Ben AR, Ridha E, Mourad Z. Detection and classification of dental caries in x-ray images using deep neural networks. Eleventh Int Conf Softw Eng Adv 2016:223-227.

25. Srivastava MM, Kumar P, Pradhan L, Varadarajan S. Detection of Tooth caries in Bitewing Radiographs using Deep Learning 2017; arXiv e-print:[arXiv:1711.07312 p.]. Available from: https://arxiv.org/abs/1711.07312.

26. Choi J, Eun H, Kim C. Boosting proximal dental caries detection via combination of variational methods and convolutional neural network. J Signal Process Sys 2018;90:87-97.

27. Lee JH, Kim DH, Jeong SN, Choi SH. Detection and diagnosis of dental caries using a deep learning-based convolutional neural network algorithm. Journal of Dentistry 2018;77:106-111.

28. Lee JH, Kim DH, Jeong SN, Choi SH. Diagnosis and prediction of periodontally compromised teeth using a deep learning-based convolutional neural network algorithm. J Periodontal Implan 2018;48:114-123.

29. Murata M, Ariji Y, Ohashi Y, Kawai T, Fukuda M, Funakoshi T,

et al. Deep-learning classification using convolutional neural network for evaluation of maxillary sinusitis on panoramic radiography. Oral Radiol 2018;35:301-307.

30. Hiraiwa T, Ariji Y, Fukuda M, Kise Y, Nakata K, Katsumata A, et al. A deep-learning artificial intelligence system for assessment of root morphology of the mandibular first molar on panoramic radiography. Dentomaxillofac Rad 2019;48:1-7.

31. Leo LM, Simla AJ. 2D to 3D conversion of dental images using deep neural network. Journal of Chemical and Pharmaceutical Sciences 2017;10:1432-1436.

32. Lee JS, Adhikari S, Liu L, Jeong HG, Kim H, Yoon SJ. Osteoporosis detection in panoramic radiographs using a deep convolutional neural network-based computer-assisted diagnosis system: a preliminary study. Dentomaxillofac Rad 2019;48:1-8.

33. Hwang JJ, Jung YH, Cho BH, Heo MS. An overview of deep learning in the field of dentistry. Imaging Sci Dent 2019;49:1-7.

34. Ariji Y, Yanashita Y, Kutsuna S, Muramatsu C, Fukuda M, Kise Y, et al. Automatic detection and classification of radiolucent lesions in the mandible on panoramic radiographs using a deep learning object detection technique. Oral Surg Oral Med Oral Pathol 2019;128:424-430.

35. Poedjiastoeti W, Suebnukarn S. Application of convolutional neural network in the diagnosis of jaw tumors. Healthc Inform Res

2018;24:236–241.

36. Ohashi Y, Ariji Y, Katsumata A, Fujita H, Nakayama M, Fukuda M, et al. Utilization of computer-aided detection system in diagnosing unilateral maxillary sinusitis on panoramic radiographs. Dentomaxillofac Radiol 2016;45:1–5.

37. Shrout MK, Hall JM, Hiideboit CE. Differentiation of periapical granulomas and radicular cysts by digital radiometric analysis. Oral Surg Oral Med Oral Pathol 1993;76: 356–361. https://doi.org/10.1016/0030-4220(93)90268-9

38. White SC, Sapp JP, Seto BG, Mankovich NI. Absence of radiometric differentiation between periapical cysts and granulomas. Oral Surg Oral Med Oral Pathol 1994;78:650–654. https://doi.org/10.1016/0030-4220(94)90180-5

39. Daley TD, Wysocki GP, The small dentigerous cyst: A diagnostic dilemma. Oral Surg Oral Med Oral Pathol 1995;17:77–81. https://doi.org/10.1016/S1079-2104(05)80078-2

40. J. Lustmann, L. Bodner. Dentigerous cysts associated with supernumerary teeth. Int. J Oral Maxillofac Surg 1988;17:100–102. https://doi.org/10.1016/S0901-5027(88)80159-0

41. Haring JI, Van Dis ML, Odontogenic keratocysts: A clinical, radiographic, and histopathologic study. Oral Surg Oral Med Oral Pathol 1988;66:145–153. https://doi.org/10.1016/0030-4220(88)90082-5

42. Ahlfors E, Larsson A, Sjggren S, The odontogenic keratocyst: A benign cystic tumor?, J Oral Maxill Surg 1984;42:10–19.

https://doi.org/10.1016/0278-2391(84)90390-2

43. Eversole LR, Leider AS,Strub D. Radiographic characteristics of cystogenic ameloblastoma. Oral Surg Oral Med Oral Pathol 1984;57:572–577. https://doi.org/10.1016/0030-4220(84)90320-7

44. Ueno S,Mushimoto K, Shirasu R. Prognostic evaluation of ameloblastoma based on histologic and radiographic typing. J Oral Maxill Surg 1989;47:11–15. https://doi.org/10.1016/0278-2391(89)90116-X

45. Ueno S, Nakamura S, Mushimoto K, Shirasu R. A Clinicopathologic Study of ameloblastoma. J Oral Maxill Surg 1986;44:361–365. https://doi.org/10.1016/S0278-2391(86)80031-3

46. Schindelin J, Arganda–Carreras I, Frise E, Kaynig V, Longair M, Pietzsch T, et al. Fiji: an open–source platform for biological–image analysis. Nat Methods 2012;9:676–682.

47. Lin TY, Dollár P, Girshick R, He K, Hariharan B, Belongie S. Feature pyramid networks for object detection. Proceedings of the IEEE conference on computer vision and pattern recognition 2017:2117–25.

48. Redmon J, Farhadi A. YOLOv3: An Incremental Improvement 2018; arXiv e–print:[arXiv:1804.02767 p.]. Available from: https://arxiv.org/abs/1804.02767.

49. Szegedy C, Toshev A, Erhan D. Deep neural networks for object detection. Advances in neural information processing systems 2013:2553–2561.

50. Girshick R, Donahue J, Darrell T, Malik J. Rich feature

hierarchies for accurate object detection and semantic segmentation. Proceedings of the IEEE conference on computer vision and pattern recognition 2014:580－587.

51. Deng XY, Liu Q, Deng Y, Mahadevan S. An improved method to construct basic probability assignment based on the confusion matrix for classification problem. Inform Sciences 2016;340:250－261.

52. Metz CE. Basic principles of roc analysis. Semin Nucl Med. 1978;8:283－298.

53. Scholl RJ, Kellett HM, Neumann DP, Lurie AG. Cysts and cystic lesions of the mandible: Clinical and radiologic－histopathologic review. Radiographics 1999;19:1107－1124.

54. Tsukamoto G, Sasaki A, Akiyama T, Ishikawa T, Kishimoto K, Nishiyama A, et al. A radiologic analysis of dentigerous cysts and odontogenic keratocysts associated with a mandibular third molar. Oral Surg Oral Med Oral Pathol 2001;91:743－747.

55. Eversole LR, Leider AS, Strub D. Radiographic characteristics of cystogenic ameloblastoma. Oral Surg Oral Med Oral Pathol 1984;57:572－577.

56. Yosinski J, Clune J, Bengio Y, Lipson H. 2014. How transferable are features in deep neural networks? Advances in neural information processing systems 3320－3328

57. Zeiler MD, Fergus R. 2014. Visualizing and understanding convolutional networks. European conference on computer vision

818-833.

58. Kohavi R. 1995. A study of cross-validation and bootstrap for accuracy estimation and model selection. Ijcai 14:1137-1145.

59. Shorten C, Khoshgoftaar TM. A survey on image data augmentation for deep learning. Journal of Big Data 2019;6:1.

요약(국문초록)

1. 목 적

 구강악안면영역에서 발생하는 낭종 혹은 종양을 조기에 발견하지 못하여 적절한 치료가 이루어지지 못하고 지연되는 경우가 있다. 이러한 문제를 해결하기 위하여 인공신경망을 기반으로 하는 기계학습 기술인 딥러닝신경망(deep convolutional neural network)을 이용하는 컴퓨터 보조진단은 보다 정확하고 빠른 결과를 제공할 수 있다. 따라서 본 연구에서는 파노라마방사선영상에서 딥러닝신경망을 이용하여 구강악안면에서 자주 나타나는 4가지 질환(함치성낭, 치근단낭, 치성각화낭, 법랑모세포종)을 자동으로 검출 및 진단하는 딥러닝신경망을 개발하고 그 정확성을 평가하였다.

2. 방 법

 본 연구에서는 파노라마방사선영상에서 악골에 발생한 치성 낭과 종양을 검출하고 진단하기 위하여 YoLoV3를 기반으로 한 딥러닝신경망을 구축하였다. 1999년부터 2017년까지 서울대학교치과병원에서 조직병리학적으로 확진된 함치성낭 350례, 치근단낭 302례, 치성각화낭 300례, 법랑모세포종 230례의 환자로부터 획득한 총 1182매 파노라마방사선영상을 분석하였다. 또한 대조군으로 질환이 없는 정상 파노라마방사선영상 100매를 선택하였다. 파노라마방사선영상 데이터는 감마, 보정, 회전, 뒤집기 기법을 통하여 12배 증강되었다. 총 데이터의 60%는 훈련세트, 20%는 검증세트,

20%는 테스트세트로 사용하였다. 개발된 딥러닝신경망은 5배 교차검증(5-fold cross validation)기법을 이용하여 평가하였다. 본 연구에서 개발한 딥러닝신경망의 성능은 정확도(Accuracy), 민감도(sensitivity), 특이도(specificity) 및 ROC분석을 통한 AUC(area under the curve) 지표를 사용하여 측정하였다.

3. 결 과

본 연구에서 개발한 딥러닝신경망은 데이터 증강을 하지 않았을 때 78.2% 민감도, 93.9% 특이도, 91.3% 정확도 및 0.86의 AUC 값을 보였고 데이터 증강을 하였을 때에는 88.9% 민감도, 97.2% 특이도, 95.6% 정확도 및 0.94 AUC의 개선된 성능을 보여주었다. 함치성낭은 91.4% 민감도, 99.2% 특이도, 97.8% 정확도 및 0.96 AUC 값을 보였다. 치근단낭은 82.8% 민감도, 99.2% 특이도, 96.2% 정확도 및 0.92 AUC 값을 나타냈다. 치성각화낭은 98.4% 민감도, 92.3% 특이도, 94.0% 정확도 및 0.97 AUC 결과를 보였다. 법랑모세포종은 71.7% 민감도, 100% 특이도, 94.3% 정확도 및 0.86 AUC의 결과를 보였다. 그리고 정상적인 악골에서는 100% 민감도, 95.1% 특이도, 96.0% 정확도 및 0.97 AUC값을 각각 보였다.

4. 결 론

본 연구에서는 파노라마방사선영상에서 치성 낭과 종양을 자동으로 검출하고 진단하는 딥러닝신경망을 개발하였다. 본 연구는

파노라마방사선영상의 수가 충분하지 않았음에도 불구하고 데이터 증강

기법을 이용하여 우수한 민감도, 특이도 및 정확도 결과를 보였다. 본

연구결과를 통하여 개발된 시스템은 환자의 상기 질환을 조기에

진단하고 적절한 시기에 치료하는데 유용하다.